JOURNAL OF VIROLOGY, Dec. 2006, p. 12248–12259 Vol. 80, No. 24
0022-538X/06/$08.00+0 doi:10.1128/JVI.01201-06

Analyses of the Interaction between the Origin Binding Domain from Simian Virus 40 T Antigen and Single-Stranded DNA Provide Insights into DNA Unwinding and Initiation of DNA Replication▽

Danielle K. Reese,† Gretchen Meinke,† Anuradha Kumar,† Stephanie Moine, Kathleen Chen, James L. Sudmeier, William Bachovchin, Andrew Bohm, and Peter A. Bullock*

Department of Biochemistry, Tufts University School of Medicine, Boston, Massachusetts 02111

Received 8 June 2006/Accepted 12 September 2006

DNA helicases are essential for DNA metabolism; however, at the molecular level little is known about how they assemble or function. Therefore, as a model for a eukaryotic helicase, we are analyzing T antigen (T-ag) the helicase encoded by simian virus 40. In this study, nuclear magnetic resonance (NMR) methods were used to investigate the transit of single-stranded DNA (ssDNA) through the T-ag origin-binding domain (T-ag OBD). When the residues that interact with ssDNA are viewed in terms of the structure of a hexamer of the T-ag OBD, comprised of residues 131 to 260, they indicate that ssDNA passes over one face of the T-ag OBD and then transits through a gap in the open ring structure. The NMR-based conclusions are supported by an analysis of previously described mutations that disrupt critical steps during the initiation of DNA replication. These and related observations are discussed in terms of the threading of DNA through T-ag hexamers and the initiation of viral DNA replication.

DNA replication, recombination, and repair are among the cellular processes that require DNA helicases (52). Further interest in these enzymes stems from their association with numerous diseases (reviewed in references 20 and 82). Therefore, efforts are under way to establish how these ATP-dependent motors function. Recent progress in this field includes the determination of the structure of the RecBCD helicase (70) and insights into how the replicative helicases of prokaryotes (40) and eukaryotes (35, 79) function. However, at the molecular level, much remains to be determined about the mechanism(s) by which helicases separate duplex DNA into single-stranded DNA (ssDNA) (52).

A useful model system for addressing how replicative helicases assemble and function is simian virus 40 (SV40) T antigen (T-ag) (reviewed in references 11, 21, and 66). Its roles in replication include site-specific binding to the viral origin, oligomerization into a double hexamer, and initial melting of the origin (reviewed in reference 7). Upon oligomerization, it can also function as a helicase (3, 72, 74) and extensively unwind duplex DNA (16, 17, 90), provided replication protein A (RPA) (reviewed in reference 89) is also present in the reaction. However, it is not understood how T-ag oligomerizes on the origin, melts the origin flanking regions, or catalyzes the unwinding of DNA at more distal locations.

One of the main advantages of using T-ag to establish how a eukaryotic replicative helicase functions is that the structure of much of the molecule has been solved. For instance, the structure of the domain necessary for site-specific binding to the viral origin, the T-ag origin-binding domain (T-ag OBD), was solved by nuclear magnetic resonance (NMR) methods (45) and more recently by crystallography techniques (48). In addition, the C-terminal helicase domain (residues 251 to 627) was solved by X-ray diffraction (23, 44). The N-terminal J domain (residues 7 to 117), needed for replication in vivo but not in vitro, has also been solved (41). Furthermore, images of T-ag hexamers and double hexamers bound to the viral origin have been obtained from electronmicroscopy studies (63, 80, 81, 83). An additional advantage is that this molecule has been subject to extensive mutagenesis studies. Thus, it is possible to interpret the T-ag structures in terms of a wealth of previous functional studies.

Given its central role in site-specific binding to the viral origin and in subsequent initiation events, we have characterized the T-ag OBD (reviewed in reference 11) and its interactions with DNA (8, 37, 42). The recent determination of the crystal structure of residues 131 to 260 of the T-ag OBD ($OBD_{131–260}$) (48) provided considerable insights into this complex topic. This study established that the T-ag $OBD_{131–260}$ forms a left-handed spiral having six monomers per turn, and it identified a gap that may play a significant role during the unwinding of duplex DNA into ssDNA. However, previous studies provided limited information regarding the possible interaction of the T-ag $OBD_{131–260}$ with ssDNA. Therefore, we have used NMR methods to investigate the binding of the T-ag $OBD_{131–260}$ to ssDNA. When the results presented here are considered in terms of the structure of the T-ag OBD hexamer, they suggest how ssDNA is routed through the spiral and then through the rest of the double hexamer complex.

MATERIALS AND METHODS

Materials and reagents. [^{15}N]ammonium chloride was purchased from Cambridge Isotope Laboratories, Inc. Single-stranded poly$(dT)_{25}$ was from Integrated DNA Technologies (Coralville, IA). Bovine alpha thrombin was purchased from Haematologic Technologies, Inc. (Essex Junction, VT).

* Corresponding author. Mailing address: Department of Biochemistry A703, Tufts University School of Medicine, 136 Harrison Ave., Boston, MA 02111. Phone: (617) 636-0447. Fax: (617) 636-2409. E-mail: peter.bullock@tufts.edu.

† D.K.R., G.M., and A.K. contibuted equally to this work.

▽ Published ahead of print on 27 September 2006.

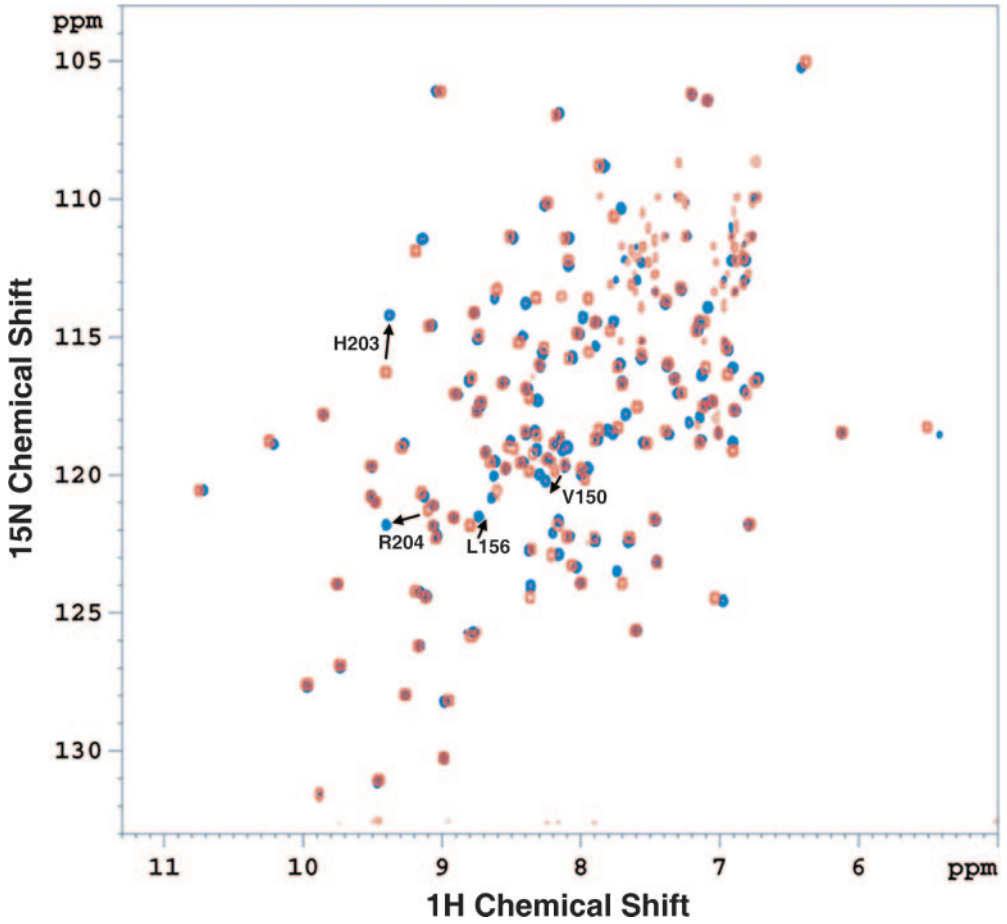

FIG. 1. Locating residues within the T-ag $OBD_{131–260}$ that bind to ssDNA via NMR methods. The 600 MHz HSQC-transverse relaxation optimized spectroscopy spectrum of a 1 mM solution of ^{15}N-labeled T-ag $OBD_{131–260}$ (Materials and Methods) at 30°C is shown in red; the assignments of the individual resonances were previously reported (45). Additional HSQC spectra were recorded as a function of increasing amounts of single-stranded poly$(dT)_{25}$ (0.1 mM to 1.5 mM); the spectrum recorded in the presence of 1.5 mM poly$(dT)_{25}$ is shown in blue. The chemical shift differences for selected residues (e.g., Val150, Leu156, His203, and Arg204) are indicated. For Val 150, the two peaks that shifted are to the left of the arrow.

Purification of the T-ag $OBD_{131–260}$. The vector used to express the T-ag $OBD_{131–260}$, pGEX T-ag OBD, was previously described (37). BL21 cells containing pGEX T-ag OBD were grown at 37°C in M9 minimal medium containing 1g/liter $^{15}NH_4Cl$ to an optical density at 600 nm of 0.8. Induction and purification of the T-ag $OBD_{131–260}$ were conducted as previously reported (37, 48). To exchange the purified ^{15}N-labeled T-ag $OBD_{131–260}$ into phosphate buffer (10 mM potassium phosphate, pH 7.0, 7 mM magnesium chloride, 100 mM potassium chloride, 1 mM dithiothreitol), the sample was passed over a Sephacryl S-100 column (Amersham). The ^{15}N-labeled T-ag $OBD_{131–260}$ was concentrated to 1 mM using spin concentrators (Viva Spin; 5,000 molecular weight cutoff).

DNA preparation. Single-stranded poly$(dT)_{25}$ (Integrated DNA Technologies) was dissolved in H_2O to 1 mM; the concentration was verified via UV absorbance at A_{260}. Aliquots (0.1 mmole) were then dried in a Speed-Vac SC100 evaporator (Savant). For a given titration point, the appropriate number of aliquots was then dissolved into the ^{15}N-labeled T-ag $OBD_{131–260}$ sample.

NMR studies. Spectra of the 1 mM sample of ^{15}N-labeled T-ag $OBD_{131–260}$ were obtained at 600 MHz on a Bruker DRX 600 spectrometer at 30°C. Dilute hydrochloric acid was used to adjust the pH of the samples to 5.5. The two-dimensional $^1H/^{15}N$ correlation between the amide protons and the covalently bound nitrogen atoms was determined by heteronuclear single-quantum coherence (HSQC)-transverse relaxation optimized spectroscopy (55) using previously described parameters (8). After an initial spectrum of the T-ag $OBD_{131–260}$ was obtained, DNA was titrated in over a range of concentrations, from 0.1 mM to 1.5 mM, and additional spectra were collected. The SPARKY assignment and integration program (University of California-San Francisco) was used to overlay spectra and determine chemical shift changes for each peak.

Molecular modeling. The coordinates for the spiral structure of the T-ag $OBD_{131–260}$ were previously reported (Protein Data Bank accession code 2FUF). Visualization of residues within the T-ag OBD was performed using the computer program VMD (NIH resource for macromolecular modeling and bioinformatics) or by PyMOL.

RESULTS

Mapping the residues within the T-ag OBD that interact with ssDNA. Previous studies revealed that T-ag binds to ssDNA in a sequence-independent manner (6, 73). However, whether ssDNA interacts with the T-ag OBD is controversial. For example, binding of the purified T-ag $OBD_{131–260}$ to ssDNA was not detected in previous electrophoretic mobility shift assay experiments (37). In contrast, residues in the A1 and B2 elements of the T-ag OBD were shown to participate in binding to helicase substrates containing ssDNA (69). Moreover, it was reported that a significant portion of the ssDNA-binding activity of T-ag may reside in the T-ag OBD although additional determinants for binding to ssDNA were suggested to lie outside of this region (49, 91). Binding of ssDNA to several domains in T-ag may help to explain the failure to

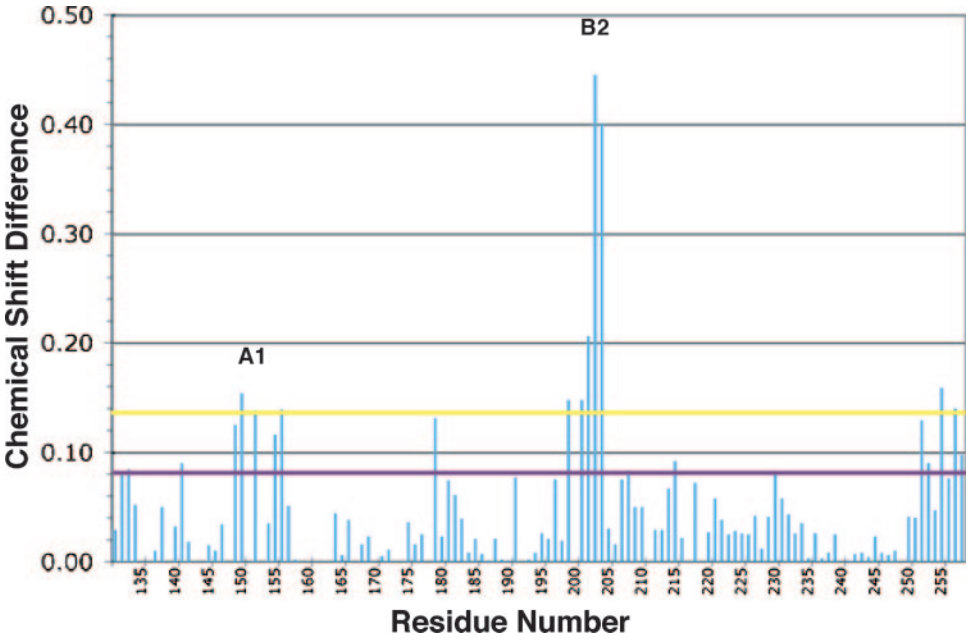

FIG. 2. Chemical shift changes in the amide backbone resonances of the T-ag $OBD_{131–260}$ after binding to 1.5 mM $poly(dT)_{25}$. The chemical shift changes were measured using the program Sparky (Materials and Methods) and plotted as a function of residue number. The largest changes were observed in the A1 (residues 147 to 159) and B2 (residues 203 to 207) regions and in the C terminus (252 to 260) (67). Chemical shift changes greater than 1 standard deviation are above the purple line, while those greater than 2 standard deviations are above the yellow line. Finally, residue 259 is a proline and does not contribute a peak to the spectrum. Therefore, data in the graph extend up to asparagine 258.

detect the interaction of the purified T-ag $OBD_{131–260}$ with ssDNA in previous experiments (37).

(i) NMR-based studies of the interaction of the T-ag $OBD_{131–260}$ with ssDNA. To clarify this issue, NMR methods were employed to assay for possible interactions between ssDNA and the T-ag $OBD_{131–260}$. A series of HSQC experiments (Materials and Methods) were performed in the presence of ^{15}N-labeled T-ag $OBD_{131–260}$ and single-stranded $poly(dT)_{25}$ (Fig. 1). The red peaks in Fig. 1 represent the HSQC spectra of the ^{15}N-labeled T-ag $OBD_{131–260}$ in the absence of ssDNA; the peak assignments were previously reported (45). Additional spectra were taken in the presence of increasing amounts of $poly(dT)_{25}$; the blue peaks represent the spectrum of ^{15}N-labeled T-ag $OBD_{131–260}$ recorded in the presence of 1.5 mM ssDNA.

The changes in the chemical shifts revealed that ssDNA has a very significant effect on selected residues (Fig. 1, arrows) within the T-ag $OBD_{131–260}$. The magnitude of the ssDNA-dependent change in the chemical shift of each residue upon the introduction of 1.5 mM of $poly(dT)_{25}$, is presented in Fig. 2. The largest chemical shift differences cluster in the B2 region (residues 203 to 207) (67); however, additional changes were observed in the A1 region (residues 147 to 159) and perhaps in the unstructured C terminus (residues 252 to 260) (45). For subsequent analyses, the chemical shift differences were broken down into two categories: those between 1 and 2 standard deviations (Fig. 2) and those above 2 standard deviations (Fig. 2).

(ii) The affinity of the T-ag $OBD_{131–260}$ for ssDNA. The HSQC titrations can also be used to estimate the affinity between substrates and ligands (30). Tight binding interactions generally have exchange rates in the slow or intermediate NMR time scale. Residues showing characteristics of slow exchange do not appear to titrate, but, rather, the intensity of the starting peak decreases as a new peak appears and increases in intensity. The interaction of the T-ag $OBD_{131–260}$ with GAGGC containing duplex DNA was in slow exchange, an indication of relatively tight binding (8). In contrast, molecules engaged in weak interactions are usually in fast exchange. During fast exchange, the observed peak is at the average position of free and bound; therefore, residues titrate as ligand is added. A representative ^{15}N stack plot for T-ag $OBD_{131–260}$ residue H203, as a function of poly(dT) addition, is shown in Fig. 3A. This residue shows a clear progression during the titration of $poly(dT)_{25}$ that is characteristic of fast exchange. The same conclusion was drawn based on a similar analysis of residue R204 (data not shown).

To extend these observations, the chemical shift data presented in Fig. 3A were used to calculate the K_d value for the interaction of the T-ag $OBD_{131–260}$ with $poly(dT)_{25}$. These analyses led to an estimated K_d value of ~25 μM (the calculation is given in the legend to Fig. 3B). This value is considerably weaker than the K_d value for the interaction of the T-ag $OBD_{131–260}$ with duplex DNA containing GAGGC sequences (31 nM when measured by fluorescence spectroscopy [78] or ~100 nM when measured by NMR [8]). Collectively, these analyses suggest that upon unwinding of the viral origin, the T-ag $OBD_{131–260}$ has a relatively weak affinity for ssDNA, a useful property for a helicase domain that must make repeated interactions with ssDNA.

(iii) Molecular modeling of the NMR-based path for ssDNA over the surface of the T-ag $OBD_{131–260}$. Several observations

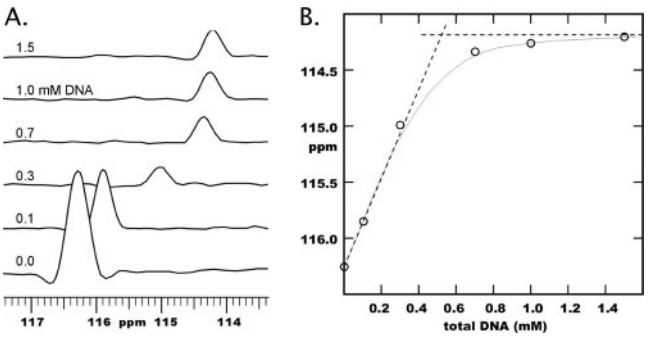

FIG. 3. ^{15}N chemical shift data of His203 used to estimate the affinity of the T-ag $OBD_{131–260}$ for ssDNA. (A) ^{15}N projections taken through the ^{15}N-^{1}H HSQC resonance of His203 in a T-ag $OBD_{131–260}$-containing solution as $poly(dT)_{25}$ was added incrementally from bottom to top. Free and bound T-ag $OBD_{131–260}$ resonances are in fast exchange, sliding gradually from left to right. The higher molecular weight of the complex leads also to smaller integrated peak areas, and some precipitation was also observed. Indeed, we estimated that the T-ag $OBD_{131–260}$ concentration fell from an initial value of nearly 1.0 mM to ~0.5 mM after the addition of the second $poly(dT)_{25}$ increment. (B) Plot of ^{15}N chemical shifts shown in panel A versus the total concentration of $poly(dT)_{25}$ DNA added. Assuming a 1:1 stoichiometry, a K_d value of 2.5×10^{-5} M is estimated. This is derived from the extrapolated value of 0.5 mM total $poly(dT)_{25}$ at the point where the T-ag $OBD_{131–260}$ should be fully bound and that ~80% of the T-ag $OBD_{131–260}$ is complexed at 0.5 mM total DNA. (Note that the concentration of free T-ag $OBD_{131–260}$ or DNA is therefore 0.2×0.5 mM = 1×10^{-4} M). It follows that K_d = [T-ag OBD][DNA]/[complex] = $(1 \times 10^{-4})\ (1 \times 10^{-4})/(4 \times 10^{-4}) = 2.5 \times 10^{-5}$ M.

indicate that the T-ag OBD can form a hexameric ring. For instance, recent crystallographic studies of the purified T-ag $OBD_{131–260}$ established that it formed a left-handed spiral, having six monomers per turn, with $P6_5$ symmetry (48). Furthermore, electronmicroscopic images of T-ag have provided additional evidence for hexameric T-ag OBD rings (81, 83). Therefore, the data in Fig. 1 were used to map the binding surface for ssDNA on the recently determined T-ag OBD hexamer (Fig. 4). In conjunction with previous mutagenesis studies (86), the recent crystallographic results (48) identified the surface of the T-ag OBD hexamer that abuts the helicase domain. The "helicase-proximal" surface contains the previously described A1 and B2 binding elements. They also established the surface that is involved in "hexamer-hexamer" interactions.

The residues that shifted in the presence of 1.5 mM $poly(dT)_{25}$ on the helicase-proximal surface (48) are depicted on the image in Fig. 4A. As previously observed (Fig. 2), many of the stronger chemical shift differences were assigned to residues (in yellow) situated in the A1 and B2 motifs. (As previously observed (Fig. 2), many of the stronger chemical shift differences were assigned to residues (in yellow) situated in the A1 and B2 motifs. Moreover, positive charges cluster in the interior of the T-ag OBD hexamer (48). Therefore, the inner surface of a given T-ag OBD hexamer would support binding of negatively charged DNA in a circular path. The residues that shifted on the opposite surface (i.e., those present in the hexamer-hexamer interface [48]) are depicted in Fig. 4B. It is apparent that there is little evidence that ssDNA interacts with this surface. Expanded views of the monomers, showing the locations of individual residues that shifted as a function of the addition of $poly(dT)_{25}$, are presented in the lower figures.

(iv) Support for the proposed path for ssDNA over the T-ag OBD derived from previous mutagenesis studies. Extensive mutagenesis studies of T-ag have been conducted (reviewed in reference 61). As a result, regions of the molecule involved in diverse activities, such as origin recognition, DNA unwinding, helicase activity, and binding to ssDNA have been identified. Therefore, to extend our studies, the replication-defective mutations within the T-ag OBD were tabulated, along with information regarding the step(s) in the initiation process that were defective in the individual mutants (Fig. 5 and 6).

Of particular interest, residues in the A1 and B2 elements (i.e., 149, 159, and 203) were reported to be necessary for binding to ssDNA containing helicase substrates (69). In addition, two neighboring residues in the T-ag OBD have been implicated in binding to ssDNA (i.e., S185 and H187) (69). In Fig. 7, T-ag OBD residues implicated in binding to ssDNA are shown in blue (the helicase-proximal surface is presented in the left panel, while the hexamer-hexamer interface is presented in the right panel). As with the HSQC experiments (Fig. 1, 2, and 4), the mutants defective for binding to the ssDNA substrates cluster, in general, on the helicase-proximal surface of the T-ag OBD hexamer. The S185 and H187 residues are, however, essentially buried and thus provide little insight. Nevertheless, the data presented in Fig. 7 supports the hypothesis that residues that bind to ssDNA are located on the helicase-proximal side of the T-ag OBD hexamer in what may be considered a circular path. Finally, it is noted that the diameter of the T-ag $OBD_{131–260}$ central channel is ~ 30 Å (48). Therefore, the circumference would be approximately 94 Å, a surface that could accommodate roughly 28 nucleotides of ssDNA.

(v) Evidence for transit of ssDNA through the gap region in the T-ag OBD hexamer. The T-ag $OBD_{131–260}$ formed an open ring hexamer whose termini fail to align (48). Therefore, upon oligomerization on the origin, a gap may be a feature of T-ag hexamers and double hexamers. A gap has also been reported to be a feature of the minichromosome maintenance complex from *Methanobacterium thermoautotrophicum* (28). The studies summarized in Fig. 8 indicate that the path for ssDNA over the T-ag OBD hexamer may include residues situated in the vicinity of the gap.

As shown in Fig. 8A, the T-ag OBD spiral hexamer is configured such that many of the A1 and B2 residues that interact preferentially with ssDNA in the NMR studies (Fig. 2) are exposed in the vicinity of the gap, particularly on the f subunit (Fig. 8A, right). In addition, many previously described replication defective mutations (Fig. 5 and 6) cluster in the region near the gap (Fig. 8B). Of particular interest, many residues that disrupt T-ag's helicase (green) and unwinding (orange) activities when mutated occur in or near the gap (Fig. 8C). The mutant data may, however, also reflect that particular residues are involved in additional activities that do not directly involve the gap (e.g., in oligomerization). Nevertheless, mutant C216G has been reported to be defective only in T-ag's single-strand-dependent unwinding activities (Fig. 6). Moreover, several mutants are defective only in T-ag's DNA binding or unwinding activities (e.g., N153S, R154S, T155S, R204K, and S219T). Therefore, since there is no indication of additional defects,

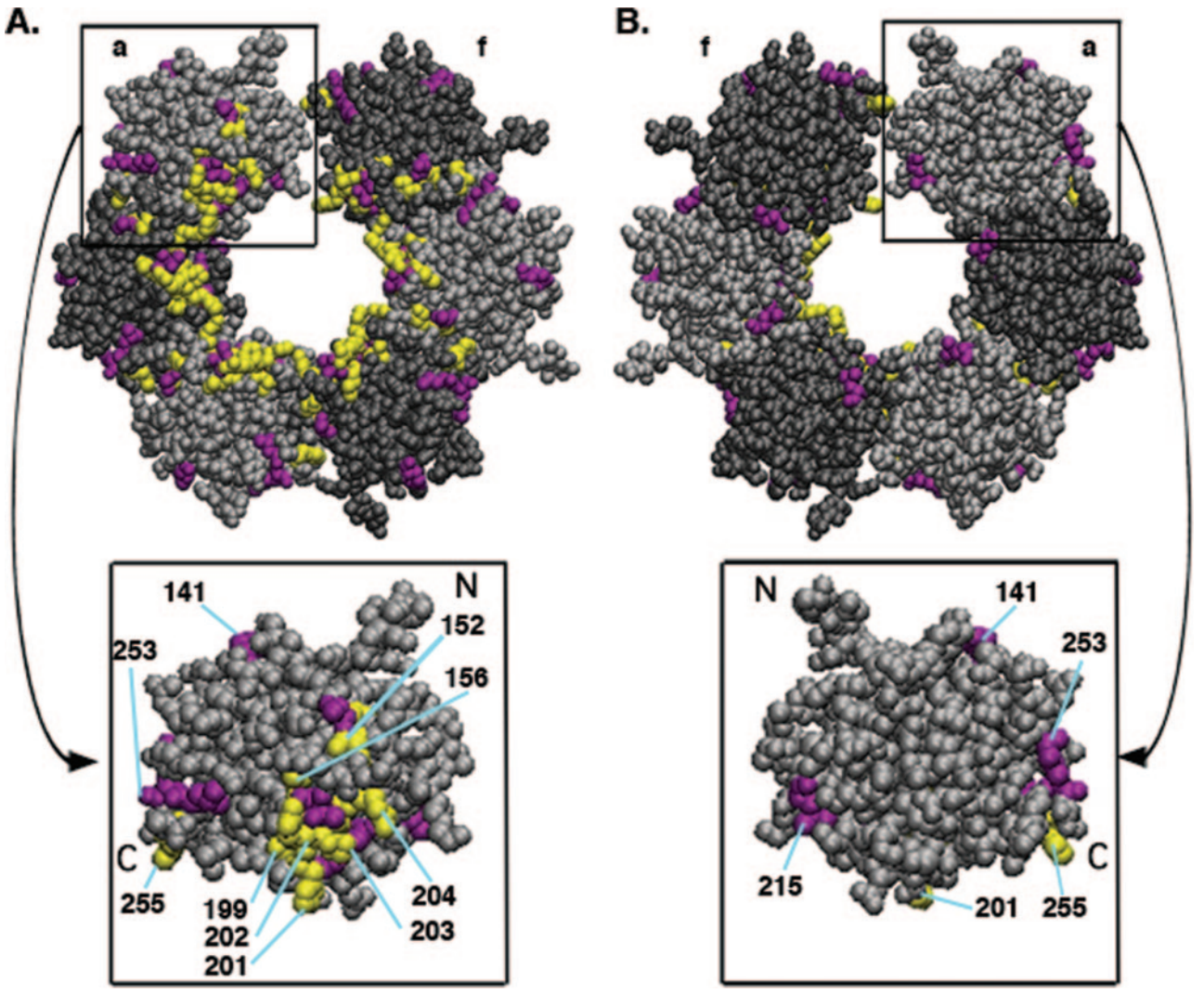

FIG. 4. Mapping residues that are involved in binding to ssDNA onto a model of a T-ag-OBD spiral hexamer. Monomers of the T-ag $OBD_{131–260}$ form a left-handed spiral with six monomers per turn (48). Two different shades of gray were used to depict the T-ag monomers, which were designated a to f. The two surfaces of the T-ag $OBD_{131–260}$ spiral were analyzed in terms of the NMR data presented in Fig. 1 and 2. (A) The helicase-proximal face of the T-ag $OBD_{131–260}$ spiral (48), with the results of the NMR studies superimposed on the surface. Residues that shifted between 1 and 2 standard deviations are shown in purple, while those that shifted greater than 2 standard deviations are shown in yellow. (B) Hexamer-hexamer interface of the T-ag $OBD_{131–260}$ spiral (48) with the residues that interacted with ssDNA mapped onto its surface. At the bottom of both panels, expanded views of the two surfaces of monomer a which identify individual residues that interacted with ssDNA. Many of the T-ag $OBD_{131–260}$ residues that shifted upon the introduction of ssDNA are derived from the A1 (residues 147 to 159) or B2 (residues 203 to 207) regions. The locations of the N terminus (N) and C terminus (C) of the T-ag $OBD_{131–260}$ are indicated.

the mutant data are consistent with the NMR-based proposal, namely, that at some point during SV40 DNA replication, ssDNA is routed past residues that are present in the vicinity of the gap.

DISCUSSION

During origin recognition, the T-ag OBD site-specifically binds to the GAGGC sequences in site II, an interaction that requires duplex DNA (reviewed in reference 11). Moreover, 1,10-phenanthroline-copper footprinting studies of T-ag double hexamers demonstrated that DNA within the T-ag OBD portion of a double hexamer is protected from cleavage (36), further evidence that within this domain, DNA is restricted to the central channel and not to the outer surfaces. Indeed, interactions between the T-ag OBD and the GAGGC pentanucleotides may anchor T-ag double hexamers to the origin prior to the initiation of helicase activity. In contrast to the evidence indicating that site II is maintained as duplex DNA, ssDNA is generated in the flanking regions in SV40 and other viral origins during initiator assembly (1, 23, 29, 36, 44, 59, 75). This has led to the hypothesis that DNA threading, particularly through the helicase domain, is coupled to assembly of T-ag on the viral origin. This possibility is supported by the observation that once hexamers and double hexamers are formed, there is no obvious mechanism for routing covalently closed circular DNA through the closed hexameric rings.

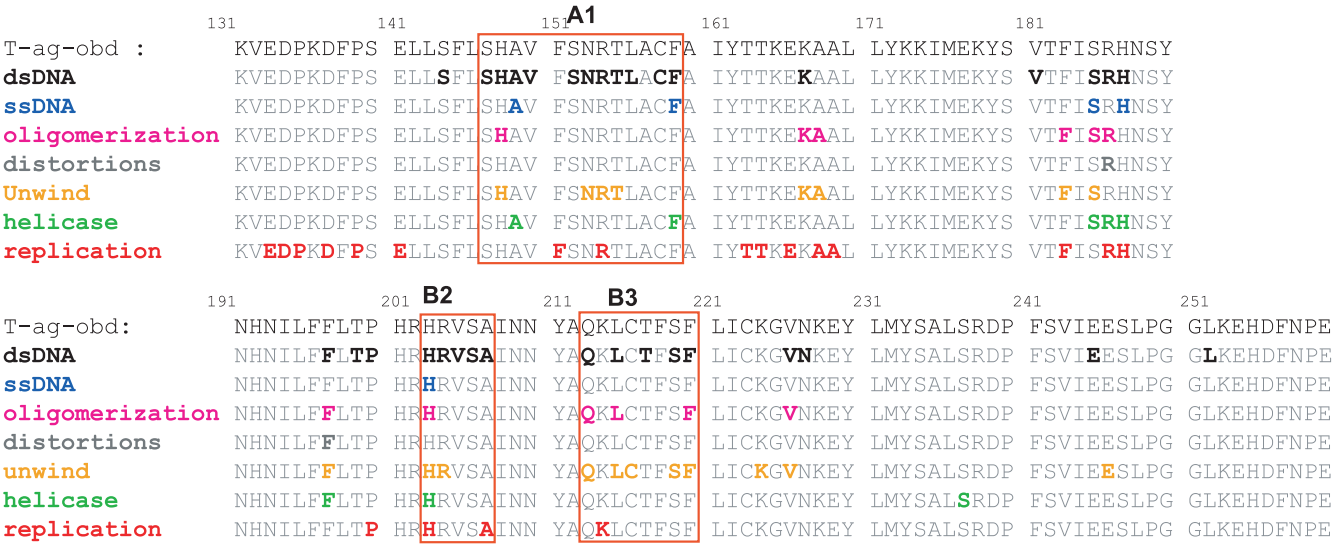

FIG. 5. The distribution of replication-defective mutations within the T-ag $OBD_{131–260}$. The top line presents the amino acid residues present in the T-ag $OBD_{131–260}$; the locations of the A1, B2, and B3 motifs (67) are indicated. The distributions of the different classes of mutants within the T-ag $OBD_{131–260}$ are displayed in the lower lines (identified by keywords). These include mutants that are defective in binding to double-stranded DNA substrates (dsDNA), binding to ssDNA, oligomerization on origin-containing DNA, DNA distortions of the origin flanking regions, the ability to unwind origin-containing DNA templates, or in their helicase activities. Finally, as noted in the legend of Fig. 6, mutants whose defects have not been determined are classified as replication defective.

When these observations are viewed in terms of our current findings, they suggest how ssDNA is routed through double hexamers assembled on the origin. A model of the T-ag OBD spiral hexamer indicating the positions of the A1 and B2 elements is shown in Fig. 9A (left); a schematic of the spiral showing the interaction of the T-ag OBD with DNA is depicted in Fig. 9A (right). A subset of the A1 and B2 elements within the spiral are proposed to bind to the GAGGC repeats in site II; however, this interaction may require structural rearrangements (48). In addition, the T-ag OBD is also able to bind to ssDNA using many of the same A1 and B2 residues used to bind to duplex DNA. Moreover, the residues that bind to ssDNA are situated on the helicase proximal face of the T-ag OBD spiral and arranged in a circular manner that terminates in the vicinity of the previously described gap (48). It is of interest that one surface of the T7 helicase/primase was also proposed to contain a circular path for ssDNA (31), and RNA may transit a surface of the open ring hexameric RNA/DNA helicase Rho in a circular manner (60). Also depicted in Fig. 9A are the locations of Glu260 (teal dashes); the linkers that connect the T-ag OBDs to the helicase domains would extend from these C-terminal residues.

A model for the passage of DNA through the entire complex is depicted in Fig. 9B. When functioning as a helicase (see below), DNA is thought to be spooled into the C termini of double hexamers formed on the origin (3, 15, 72, 88). Therefore, the black arrows indicate duplex DNA moving toward the C terminus of a given T-ag hexamer. Exactly how both strands of DNA transit through the helicase domain has yet to be established. However, based on parallels with prokaryotic helicases, such as DnaB (39, 40) and the T7 helicase (2, 31), one strand of DNA is proposed to enter the helicase domain via the central channel, while the second strand is proposed to be routed over the surface of the helicase domain. An alternative possibility is that duplex DNA enters the central channel, and then at least one strand transits to the helicase surface via the side channels (23, 29, 44, 80). Nevertheless, both models suggest that an external strand would transit past the Zn motif-containing D1 domain; thus, it is ideally situated to enter the gap present in the "lock-washer" conformation of the T-ag OBD hexamer. A similar gap is present in Rho, a prokaryotic hexameric RNA/DNA helicase (71). The gap in Rho was suggested to facilitate loading of the molecule onto single-stranded RNA. The gap in T-ag hexamers, and in other hexameric helicases needed for DNA replication, may serve the analogous function of enabling the passage of ssDNA from the central regions of these complexes. This proposal is consistent with previous electronmicroscopy studies that reported "rabbit ears" emerging from the central region of T-ag double hexamers (29, 88). Finally, it is proposed that the overall path of DNA through the second T-ag OBD hexamer is similar to that used to transit the first hexamer. However, based on the need to expose both parental strands as templates for DNA synthesis, it is likely that the complementary strand is routed through the central channel of the second hexamer. This arrangement may be related to the observation that the two hexamers appear to be rotated relative to each other (29).

Double hexamers of T-ag assembled on the core origin are stable entities that do not extensively unwind duplex DNA. However, with origin containing linear DNA substrates, DNA unwinding is detected upon the addition of RPA (17, 27). Thus, RPA is a necessary cofactor for detecting the 3′ to 5′ helicase activity of T-ag. Therefore, it is of interest that RPA binds selectively to the T-ag OBD (85). Indeed, the C terminus of the 30-kDa subunit of RPA contacts the A1 and B2 motifs at many of the same residues used to bind to ssDNA (4). This suggests that RPA competes with ssDNA for many of the same residues on the A1 and B2 motifs. Furthermore, the affinity of

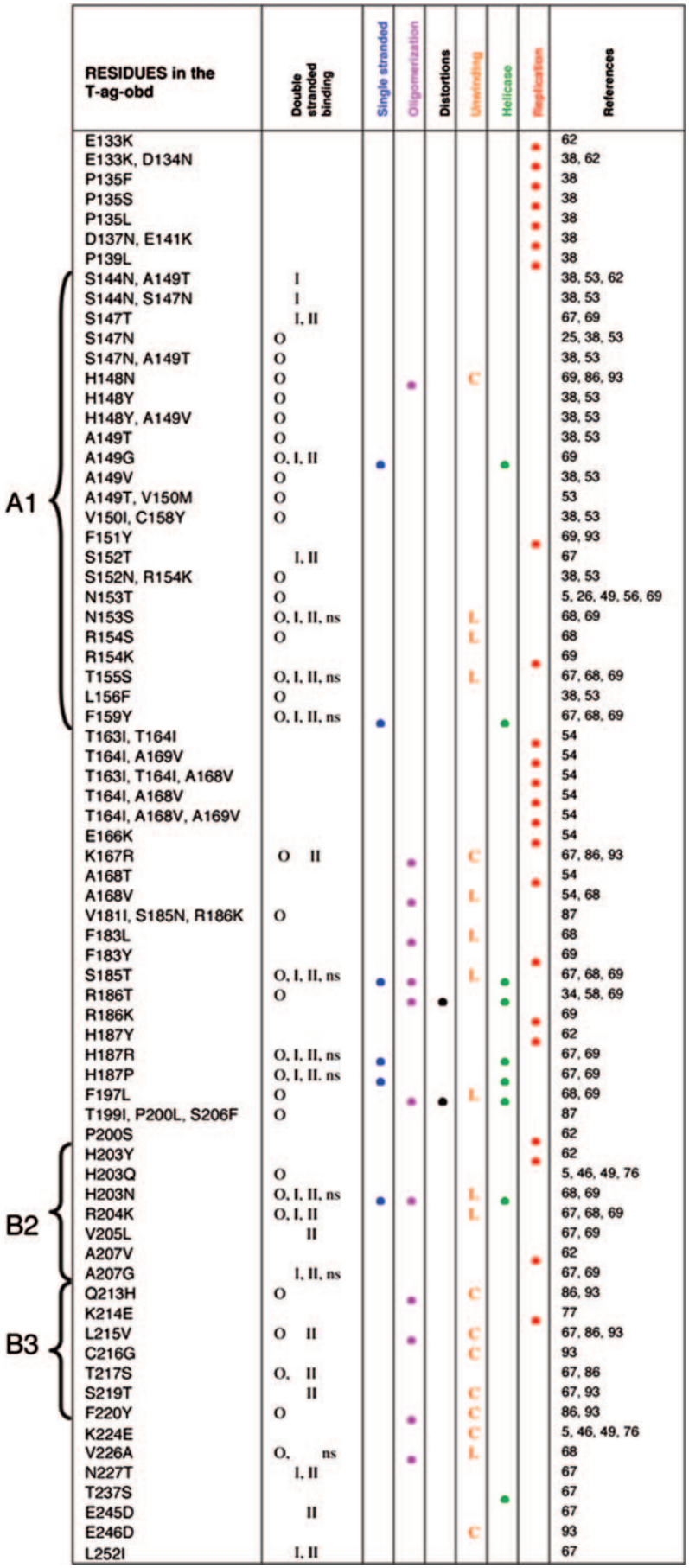
RESIDUES in the T-ag-obd
Double stranded binding
Single stranded
Oligomerization
Distortions
Unwinding
Helicase
Replication
References
A1
B2
B3
E133K 62
E133K, D134N 38, 62
P135F 38
P135S 38
P135L 38
D137N, E141K 38
P139L 38
S144N, A149T I 38, 53, 62
S144N, S147N I 38, 53
S147T I, II 67, 69
S147N O 25, 38, 53
S147N, A149T O 38, 53
H148N O 69, 86, 93
H148Y O 38, 53
H148Y, A149V O 38, 53
A149T O 38, 53
A149G O, I, II 69
A149V O 38, 53
A149T, V150M O 53
V150I, C158Y O 38, 53
F151Y 69, 93
S152T I, II 67
S152N, R154K O 38, 53
N153T O 5, 26, 49, 56, 69
N153S O, I, II, ns 68, 69
R154S O 68
R154K 69
T155S O, I, II, ns 67, 68, 69
L156F O 38, 53
F159Y O, I, II, ns 67, 68, 69
T163I, T164I 54
T164I, A169V 54
T163I, T164I, A168V 54
T164I, A168V 54
T164I, A168V, A169V 54
E166K 54
K167R O II 67, 86, 93
A168T 54
A168V 54, 68
V181I, S185N, R186K O 87
F183L 68
F183Y 69
S185T O, I, II, ns 67, 68, 69
R186T O 34, 58, 69
R186K 69
H187Y 62
H187R O, I, II, ns 67, 69
H187P O, I, II, ns 67, 69
F197L O 68, 69
T199I, P200L, S206F O 87
P200S 62
H203Y 62
H203Q O 5, 46, 49, 76
H203N O, I, II, ns 68, 69
R204K O, I, II 67, 68, 69
V205L II 67, 69
A207V 62
A207G I, II, ns 67, 69
Q213H O 86, 93
K214E 77
L215V O II 67, 86, 93
C216G 93
T217S O, II 67, 86
S219T II 67, 93
F220Y O 86, 93
K224E 5, 46, 49, 76
V226A O, ns 68
N227T I, II 67
T237S 67
E245D II 67
E246D 93
L252I I, II 67

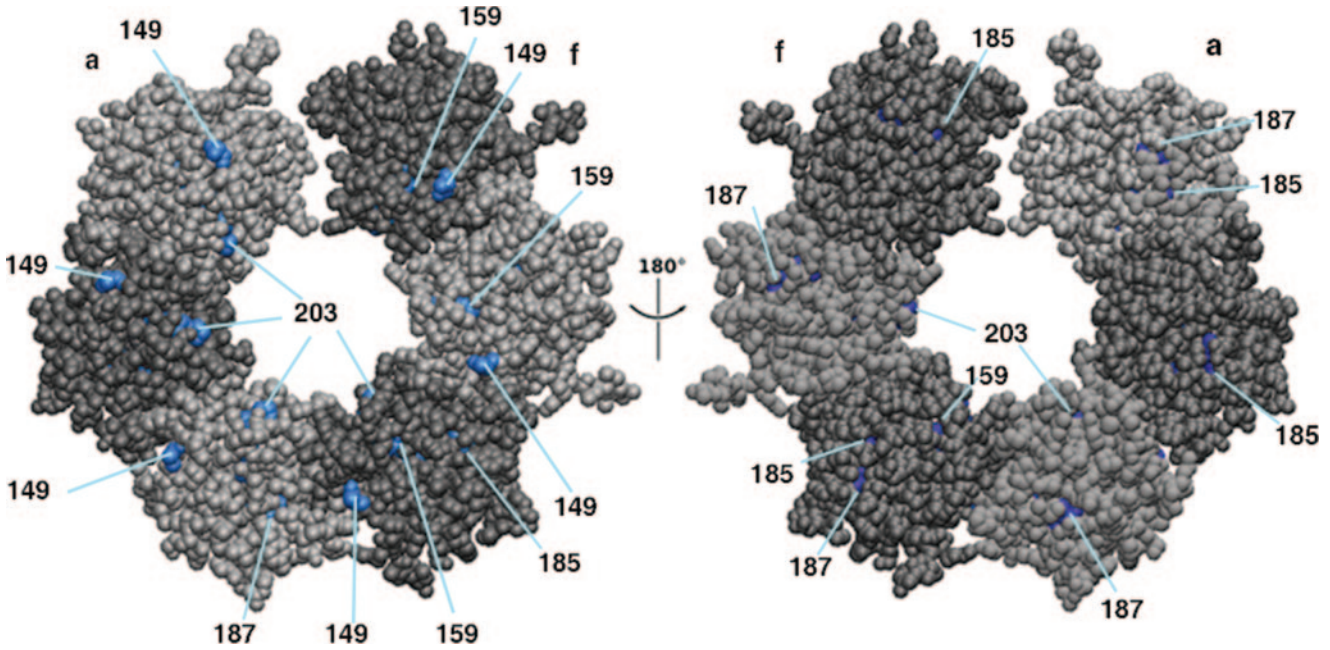

FIG. 7. Mutational-based evidence that one face of the T-ag OBD spiral contains a binding surface for ssDNA. The distribution of T-ag OBD mutations that were previously shown to be defective for binding to ssDNA containing helicase substrates (M13mp19 ssDNA to which a primer had been annealed) (69, 92) are shown in blue (i.e., A149, F159, and H203). As in Fig. 4, the individual monomers are colored in alternating shades of gray and labeled a to f. On the left is presented the helicase-proximal surface of the T-ag OBD (48); residues 149, 159, and 203 cluster on this surface. In contrast, inspection of the right-hand image reveals that atoms from these residues are not significant features of the hexamer-hexamer surface of the T-ag OBD. Finally, T-ag OBD residues S185 and H187 have also been implicated in binding to ssDNA (69). However, they are internally located; therefore, atoms from these residues can be seen on both surfaces.

RPA for ssDNA (K_d of ~0.01 to 1 nM (89) is much higher than the affinity of the T-ag $OBD_{131–260}$ for ssDNA (~25 μM). Since the A1 and B2 loops in the spiral hexamer are oriented toward the helicase domain (48), the net effect of helicase activity would be the extrusion of ssDNA out through the gap near the helicase domain and its subsequent transfer to RPA.

Regarding the T-ag-dependent forces that are needed to propel DNA through the double hexamers during unwinding, the beta-hairpins located in the helicase domains are likely to pump DNA through the center of the complex (19, 23, 44, 59, 65). However, additional forces may be operating. For example, in the vicinity of the gap the externally routed ssDNA may be constrained owing to its interactions with the A1 and B2 motifs and the linkers that connect the T-ag OBD monomers to the helicase domains. Therefore, if the helicase domain were rotated relative to the T-ag OBD domain, perhaps as a result of ATP hydrolysis or RPA binding, the ssDNA would be subjected to a ratcheting force that would promote its movement across the surface of the helicase domain.

The path taken by ssDNA through the T-ag OBD hexamer and the rest of the complex is also relevant to a consideration of how nascent DNA is synthesized in the vicinity of the viral

FIG. 6. Compilation of mutants within the T-ag OBD which are defective for DNA replication; the references to the individual mutations are presented. In many instances, the step(s) in the initiation process that are defective are known. For example, a number of mutants are defective in binding to double-stranded DNA substrates (i.e., the core origin [0], site I [I], site II [II], an origin subfragment containing pentanucleotides 1, 2, and the early palindrome [1,2+EP], and non-sequence-specific [ns] DNA). Additional mutants (identified by keywords) were defective for binding to single-stranded DNA, oligomerization on origin-containing DNA, DNA distortions of the origin flanking regions, the ability to unwind covalently closed circles (C) or linear (L) DNA, or helicase activities. However, in several instances, the stage at which the mutants are defective has not been determined. Therefore, these mutants were simply classified as replication defective. (A dot is used to symbolize that a given activity was inactivated). Within the T-ag OBD, residues in the A1 and B2 elements (147 to 159 and 203 to 207, respectively) mediate site-specific binding to the GAGGC sequences in the central, or site II, region of the origin (reviewed in references 11 and 66). Related studies led to the organization of mutations within the T-ag OBD into different classes (68, 93). Class 1, with mutations introduced at residues N153, R154, T155, F159, F197, and R204, are defective for binding to the SV40 origin of replication. Class 2, with mutations introduced at residues S185, H203, and V226, are unable to bind to DNA, either site-specifically to the origin or in a non-sequence-specific manner. In contrast, class 3, with mutations at residues A168 and F183, bind to DNA like wild-type T-ag but are unable to unwind origin-containing fragments of DNA and fail to correctly oligomerize in response to ATP. Class 4, with mutations at residues H148, K167, Q213, L215, C216, S219, F220, and E246 (93), are defective in unwinding closed circular DNA and in supporting DNA replication in vitro. Of interest, a number of the class 4 mutants (i.e., Q213, L215, C216, S219, and F220) are clustered at an interface that is thought to mediate hexamer-hexamer association (48). Class 5, with mutations at residues F151, T217, N227, and E245, support DNA replication in vitro but not in vivo. Finally, residues in T-ag OBD are also required for interactions with cellular proteins that initiate DNA synthesis. For example, the hRPA32 C-terminal domain binds to the T-ag OBD (4). Residues in the T-ag OBD that appear to be involved in this interaction include R154, H201, R202, R204, N258, and P259.

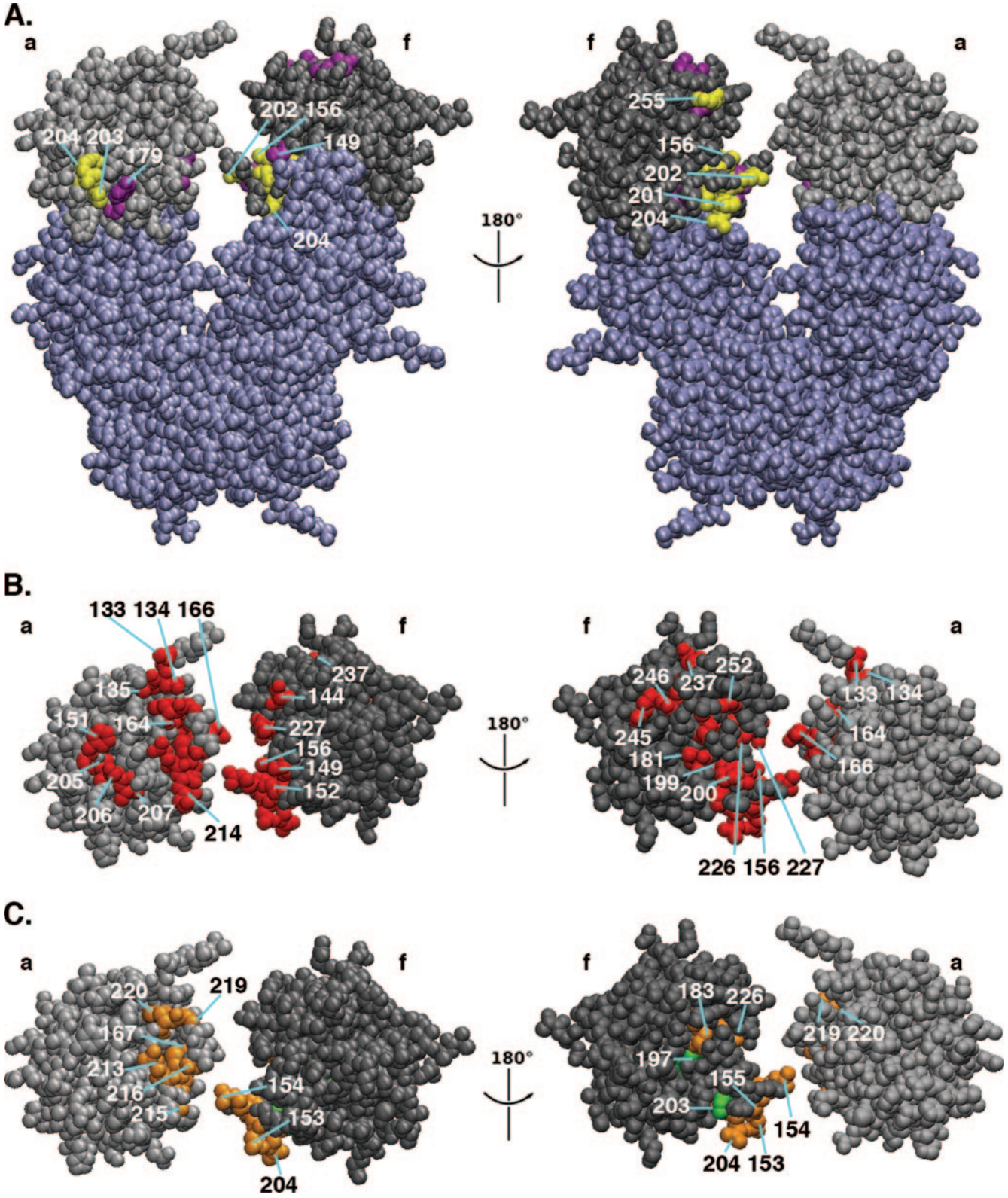

FIG. 8. Evidence that ssDNA interacts with residues situated in the gap in the T-ag OBD. (A) Two views of the T-ag OBD spiral that are related by a rotation of 180°. For simplicity, the T-ag OBD monomers that are situated such that they do not contribute residues to the terminal portion of the gap, present in monomers a and f, are shown in light blue. Residues in the terminal region of the gap that underwent significant chemical shift changes upon binding to ssDNA are colored as described in the legend of Fig. 4. (B) The distribution of previously described replication-defective mutations in the terminal region of the gap. The relevant residues that can be see from either view include E133, D134, P135, S144, A149, F151, S152, L156, T164, E166, V181, T199, P200, V205, S206, A207, K214, V226, N227, T237, E245, E246, and L252 (Fig. 5 and 6). The residues whose replication defect is in either DNA unwinding or helicase activities (see panel C) are colored, but not labeled. (C) The distribution of residues in the terminal portion of the gap that selectively disrupted either DNA unwinding (orange residues; N153, R154, T155, K167, F183, R204, Q213, L215, C216, S219, F220, and V226) or helicase activity (green residues; F197 and H203) when mutated (Fig. 5 and 6).

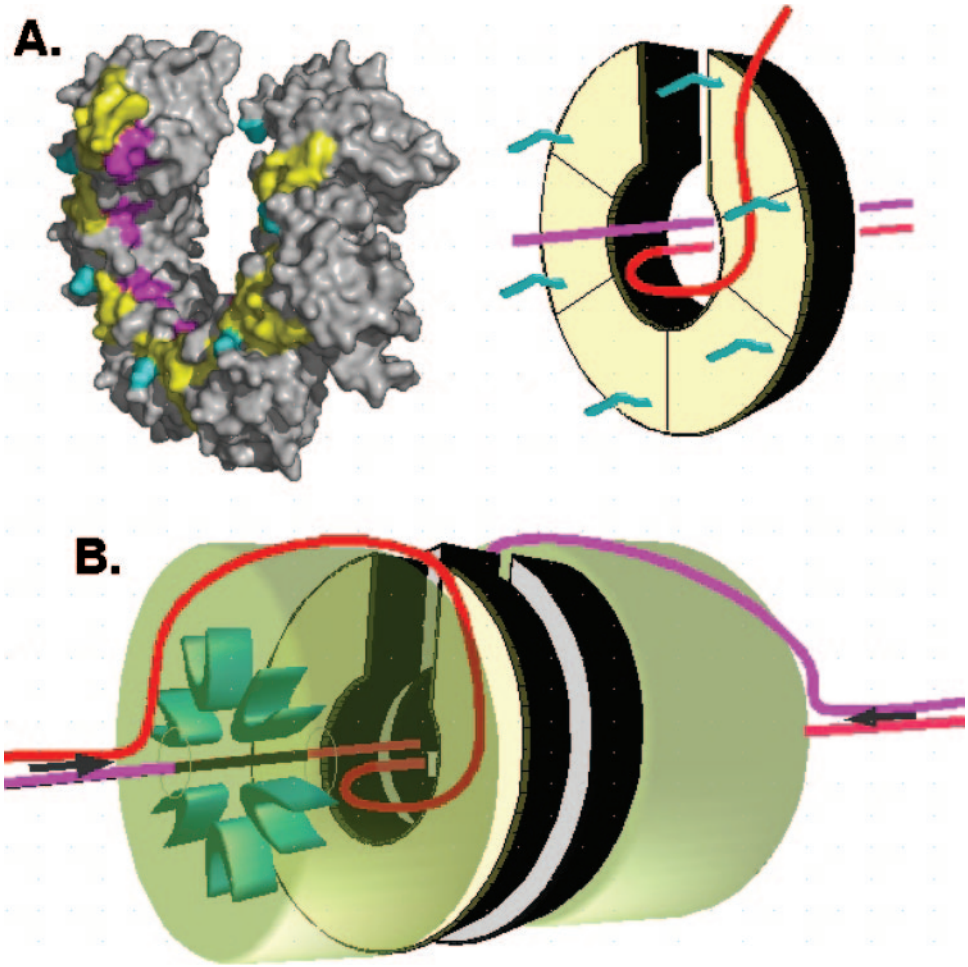

FIG. 9. A model depicting the transit of ssDNA through T-ag double hexamers assembled on the core origin. (A) Models depicting a T-ag OBD hexamer and its interactions with DNA. On the left is a model of the spiral hexamer; the gap in the lock-washer conformation is evident at the terminus. The A1 residues are shown in yellow, and the B2 residues are shown in red. T-ag OBD residue Glu260 is shown in teal; the linker that connects the T-ag OBD with the helicase domain (44) would be attached to these residues. The image to the right is a schematic of the T-ag OBD spiral, depicting the transit of DNA (pink and red strands) through the complex. The binding surface for ssDNA, comprised mainly of residues in the A1 and B2 regions, is symbolized by the yellow surface. T-ag OBD residue Glu260 is depicted by the small teal dashes. (B) A model for the transit of DNA through a T-ag double hexamer; the helicase domain is depicted in light green. The black arrows symbolize the pumping of duplex DNA into the double hexamer complex. At least one strand enters the central channel of the helicase domain, where it interacts with the beta hairpins (propeller-like structures) (23, 59, 65). Based on the transit of DNA over prokaryotic helicases (see text), the second strand is depicted going over the outer surface of the helicase domain. However, an alternative possibility is that it travels through a side channel (22, 44) and transits past only a limited amount of the external surface of the helicase domain. In either case, the externally routed strand is proposed to transit through the gap in the T-ag OBD hexamers.

origin. The polymerase α-primase complex is known to bind to the helicase domain of T-ag (18, 24) and to share with T-ag overlapping sites of interaction on the 70-kDa subunit of RPA (9). These and related observations led to the hypothesis that T-ag, RPA, and the polymerase α-primase complex form a preinitiation complex (reviewed in references 10, 11, 21, 33, 66, and 84). Based on the current findings, it is possible that upon emergence of ssDNA out of the gap in the T-ag OBD hexamer, the polymerase α-primase complex initiates primer-RNA/DNA synthesis at pyrimidine-rich trinucleotide sequences (12, 13, 50, 51, 57). Competition for RPA would then enable replication factor C to displace the polymerase α-primase complex and to load proliferating cell nuclear antigen (94). The subsequent binding of polymerase δ to both RPA and proliferating cell nuclear antigen would promote a polymerase switch (reviewed in references 35 and 84) and the establishment of the leading strand complex. It follows that the leading strand complex may be positioned where ssDNA is generated within the helicase domain.

A number of important issues regarding the interaction of the T-ag OBD with the SV40 origin remain to be clarified. For example, little is known regarding the point at which site II is unwound, and there is uncertainty regarding the exact stage at which all four pentanucleotides are bound (36, 78). Nevertheless, based on primary sequence and structural homologies (14, 32), it is likely that the interactions between the OBDs encoded by other members of the *Polyomaviridae* family of viruses and both duplex and ssDNA occur via mechanisms that

are similar to those employed by the T-ag OBD. Furthermore, the helicase domains of SV40 T-ag, papillomavirus E1, and the archaeal minichromosome maintenance complex (47) contain the beta-hairpin motif (1, 19, 44, 59, 64, 65), one indication that these domains will also interact with DNA in a related manner. Therefore, it will be of interest to determine the extent to which the transit of DNA through other hexameric helicases, such as additional members of the SF3 family of helicases (43), has been conserved.

ACKNOWLEDGMENTS

This work was supported by a grant from the National Institutes of Health to P.A.B. (9R01GM55397).

We thank Gillian D. Henry for useful discussions and Paul J. Phelan for comments on the manuscript.

Addendum in Proof

After this manuscript was submitted, Enemark and Joshua-Tor (E. J. Enemark and L. Joshua-Tor, Nature **442:**270–275, 2006) published an article that examined the mechanism of DNA translocation through the papillomavirus E1 hexameric ring helicase. In keeping with the model for SV40 T-ag presented in Fig. 9B, their experiments demonstrate that only a single strand of DNA transits through the central channel of the papillomavirus helicase domain. Their data also indicate that the ssDNA located in the central channel is translocated out of the hexameric complex. In contrast, previous studies suggested that DNA is translocated into hexameric complexes (Fig. 9B, black arrows). One consequence of this altered polarity of translocation through the T-ag double hexamer complex would be that nascent DNA synthesis would likely occur where ssDNA emerges from the C termini of the helicase domains, not in the vicinity of the gaps.

REFERENCES

1. **Abbate, E. A., J. M. Berger, and M. R. Botchan.** 2004. The X-ray structure of the papillomavirus helicase in complex with its molecular matchmaker E2. Genes Dev. **18:**1981–1996.
2. **Ahnert, P., and S. S. Patel.** 1997. Asymmetric interactions of hexameric bacteriophage T7 DNA helicase with the 5′- and 3′-tails of the forked DNA substrate. J. Biol. Chem. **272:**32267–32273.
3. **Alexandrov, A. I., M. R. Botchan, and N. R. Cozzarelli.** 2002. Characterization of simian virus 40 T-antigen double hexamers bound to a replication fork. J. Biol. Chem. **277:**44886–44897.
4. **Arunkumar, A. I., V. Klimovich, X. Jiang, R. D. Ott, L. Mizoue, E. Fanning, and W. J. Chazin.** 2005. Insights into hRPA32 C-terminal domain-mediated assembly of the simian virus 40 replisome. Nat. Struct. Mol. Biol. **12:**332–339.
5. **Auborn, K., M. Guo, and C. Prives.** 1989. Helicase, DNA-binding, and immunological properties of replication-defective simian virus 40 mutant T antigens. J. Virol. **63:**912–918.
6. **Auborn, K. J., R. B. Markowitz, E. Wang, T. Yu, and C. Prives.** 1988. Simian virus 40 (SV40) T antigen binds specifically to double-stranded DNA but not to single-stranded DNA or DNA/RNA hybrids containing the SV40 regulatory sequences. J. Virol. **62:**2204–2208.
7. **Borowiec, J. A., F. B. Dean, P. A. Bullock, and J. Hurwitz.** 1990. Binding and unwinding: how T antigen engages the SV40 origin of DNA replication. Cell **60:**181–184.
8. **Bradshaw, E. M., D. G. Sanford, X. Luo, J. L. Sudmeier, Z. A. Guard-Levin, P. A. Bullock, and W. W. Bachovchin.** 2004. T antigen origin-binding domain of simian virus 40: determinants of specific DNA binding. Biochemistry **43:**6928–6936.
9. **Braun, K. A., Y. Lao, Z. He, C. J. Ingles, and M. S. Wold.** 1997. Role of protein-protein interactions in the function of replication protein A (RPA): RPA modulates the activity of DNA polymerase α by multiple mechanisms. Biochemistry **36:**8443–8454.
10. **Brush, G. S., and T. J. Kelly.** 1996. Mechanisms for replicating DNA, p. 1–43. *In* M. L. DePamphilis (ed.), DNA replication in eukaryotic cells. Cold Spring Harbor Laboratory Press, Cold Spring Harbor, N.Y.
11. **Bullock, P. A.** 1997. The initiation of simian virus 40 DNA replication in vitro. Crit. Rev. Biochem. Mol. Biol. **32:**503–568.
12. **Bullock, P. A., Y. S. Seo, and J. Hurwitz.** 1991. Initiation of simian virus 40 DNA synthesis in vitro. Mol. Cell. Biol. **11:**2350–2361.
13. **Bullock, P. A., S. Tevosian, C. Jones, and D. Denis.** 1994. Mapping initiation sites for simian virus 40 lagging strand DNA synthesis events in vitro. Mol. Cell. Biol. **14:**5043–5055.
14. **Campos-Olivas, R., J. M. Louis, D. Clerot, B. Gronenborn, and A. M. Gronenborn.** 2002. The structure of a replication initiator unites diverse aspects of nucleic acid metabolism. Proc. Natl. Acad. Sci. USA **99:**10310–10315.
15. **Cook, P. R.** 1999. The organization of replication and transcription. Science **284:**1790–1795.
16. **Dean, F. B., P. Bullock, Y. Murakami, C. R. Wobbe, L. Weissbach, and J. Hurwitz.** 1987. Simian virus 40 (SV40) DNA replication: SV40 large T antigen unwinds DNA containing the SV40 origin of replication. Proc. Natl. Acad. Sci. USA **84:**16–20.
17. **Dodson, M., F. B. Dean, P. Bullock, H. Echols, and J. Hurwitz.** 1987. Unwinding of duplex DNA from the SV40 origin of replication by T antigen. Science **238:**964–967.
18. **Dornreiter, I., L. F. Erdile, I. U. Gilbert, D. von Winkler, T. J. Kelly, and E. Fanning.** 1992. Interactions of DNA polymerase α-primase with cellular replication protein A and SV40 T antigen. EMBO J. **11:**769–776.
19. **Enemark, E. J., and L. Joshua-Tor.** 2006. Mechanism of DNA translocation in a replicative hexameric helicase. Nature **442:**270–275.
20. **Epstein, C. J., and A. G. Motulsky.** 1996. Werner syndrome: entering the helicase era. BioEssays **18:**1025–1027.
21. **Fanning, E., and R. Knippers.** 1992. Structure and function of simian virus 40 large tumor antigen. Annu. Rev. Biochem. **61:**55–85.
22. **Gai, D., D. Li, C. V. Finkielstein, R. D. Ott, P. Taneja, E. Fanning, and X. S. Chen.** 2004. Insights into the oligomeric states, conformational changes and helicase activities of SV40 large tumor antigen. J. Biol. Chem. **279:**38952–38959.
23. **Gai, D., R. Zhao, D. Li, C. V. Finkielstein, and X. S. Chen.** 2004. Mechanisms of conformational change for a replicative hexameric helicase of SV40 large tumor antigen. Cell **119:**47–60.
24. **Gannon, J. V., and D. P. Lane.** 1987. p53 and DNA polymerase α compete for binding to SV40 T antigen. Nature (London) **329:**456–458.
25. **Gish, W. R., and M. R. Botchan.** 1987. Simian virus 40-transformed human cells that express large T antigens defective for viral DNA replication. J. Virol. **61:**2864–2876.
26. **Gluzman, Y., and B. Ahrens.** 1982. SV40 early mutants that are defective for viral DNA synthesis but competent for transformation of cultured rat and simian cells. Virology **123:**78–92.
27. **Goetz, G. S., F. B. Dean, J. Hurwitz, and S. W. Matson.** 1988. The unwinding of duplex regions in DNA by the simian virus 40 large tumor antigen-associated DNA helicase activity. J. Biol. Chem. **263:**383–392.
28. **Gomez-Llorente, Y., R. J. Fletcher, X. S. Chen, J. M. Carazo, and C. SanMartin.** 2005. Polymorphism and double hexamer structure in the archaeal minichromosome maintenance (MCM) helicase from *Methanobacterium thermoautotrophicum*. J. Biol. Chem. **280:**40909–40915.
29. **Gomez-Lorenzo, M. G., M. Valle, L. E. Donate, C. Gruss, C. O. S. Sorzano, M. Radermacher, J. Frank, and J. M. Carazo.** 2003. Large T antigen on the SV40 origin of replication: a 3D snapshot prior to DNA replication. EMBO J. **22:**6205–6213.
30. **Gunther, U., and B. Schaffhausen.** 2002. NMRKIN: Simulating line shapes from two-dimensional spectra of proteins. J. Biomol. NMR **22:**201–209.
31. **Hacker, K. J., and K. A. Johnson.** 1997. A hexameric helicase encircles one DNA strand and excludes the other during DNA unwinding. Biochemistry **36:**14080–14087.
32. **Hickman, A. B., R. D. Ronning, R. M. Kotin, and R. Dyda.** 2002. Structural unity among viral origin binding proteins: crystal structure of the nuclease domain of adeno-associated virus Rep. Mol. Cell **10:**327–337.
33. **Hurwitz, J., F. B. Dean, A. D. Kwong, and S.-H. Lee.** 1990. The in vitro replication of DNA containing the SV40 origin. J. Biol. Chem. **265:**18043–18046.
34. **Hutchinson, N. I., L.-S. Chang, M. M. Pater, N. Bouck, T. E. Shenk, and G. DiMayorca.** 1985. Characterization of a new simian virus 40 mutant, tsA3900, isolated from deletion mutant tsA1499. J. Virol. **53:**814–821.
35. **Johnson, A., and M. O'Donnell.** 2005. Cellular DNA replicases: components and dynamics at the replication fork. Annu. Rev. Biochem. **74:**283–315.
36. **Joo, W. S., H. Y. Kim, J. D. Purviance, K. R. Sreekumar, and P. A. Bullock.** 1998. Assembly of T-antigen double hexamers on the simian virus 40 core origin requires only a subset of the available binding sites. Mol. Cell. Biol. **18:**2677–2687.
37. **Joo, W. S., X. Luo, D. Denis, H. Y. Kim, G. J. Rainey, C. Jones, K. R. Sreekumar, and P. A. Bullock.** 1997. Purification of the SV40 T-antigen DNA binding domain and characterization of its interactions with the SV40 origin. J. Virol. **71:**3972–3985.
38. **Kalderon, D., and A. E. Smith.** 1984. In vitro mutagenesis of a putative DNA binding domain of SV40 large-T. Virology **139:**109–137.
39. **Kaplan, D. L., M. J. Davey, and M. O'Donnell.** 2003. Mcm4,6,7 uses a "pump in ring" mechanism to unwind DNA by steric exclusion and actively translocates along a duplex. J. Biol. Chem. **278:**49171–49182.
40. **Kaplan, D. L., and M. O'Donnell.** 2004. Twin DNA pumps of a hexameric helicase provide power to simultaneously melt two duplexes. Mol. Cell **15:**453–465.
41. **Kim, H.-Y., B. Y. Ahn, and Y. Cho.** 2001. Structural basis for the inactivation

of retinoblastoma tumor suppressor by SV40 large T antigen. EMBO J. **20:**295–304.
42. **Kim, H. Y., B. A. Barbaro, W. S. Joo, A. Prack, K. R. Sreekumar, and P. A. Bullock.** 1999. Sequence requirements for the assembly of simian virus 40 T-antigen and T-antigen origin binding domain on the viral core origin of replication. J. Virol. **73:**7543–7555.
43. **Koonin, E. V.** 1993. A common set of conserved motifs in a vast variety of putative nucleic acid-dependent ATPases including MCM proteins involved in the initiation of eukaryotic DNA replication. Nucleic Acids Res. **21:**2541–2547.
44. **Li, D., R. Zhao, W. Lilyestrom, D. Gai, R. Zhang, J. A. DeCaprio, E. Fanning, A. Jochimiak, G. Szakonyl, and X. S. Chen.** 2003. Structure of the replicative helicase of the oncoprotein SV40 large tumor antigen. Nature **423:**512–518.
45. **Luo, X., D. G. Sanford, P. A. Bullock, and W. W. Bachovchin.** 1996. Structure of the origin specific DNA binding domain from simian virus 40 T-antigen. Nat. Struct. Biol. **3:**1034–1039.
46. **Manos, M. M., and Y. Gluzman.** 1985. Genetic and biochemical analysis of transformation-competent, replication-defective simian virus 40 large T antigen mutants. J. Virol. **53:**120–127.
47. **McGeoch, A. T., M. A. Trakselis, R. A. Laskey, and S. D. Bell.** 2005. Organization of the archaeal MCM complex on DNA and implications for the helicase mechanism. Nat. Struct. Mol. Biol. **12:**756–762.
48. **Meinke, G., P. A. Bullock, and A. Bohm.** 2006. Crystal structure of the simian virus 40 large T-antigen origin-binding domain. J. Virol. **80:**4304–4312.
49. **Mohr, I. J., M. P. Fairman, B. Stillman, and Y. Gluzman.** 1989. Large T-antigen mutants define multiple steps in the initiation of simian virus 40 DNA replication. J. Virol. **63:**4181–4188.
50. **Murakami, Y., T. Eki, and J. Hurwitz.** 1992. Studies on the initiation of simian virus 40 replication in vitro: RNA primer synthesis and its elongation. Proc. Natl. Acad. Sci. USA **89:**952–956.
51. **Nethanel, T., and G. Kaufmann.** 1990. Two DNA polymerases may be required for synthesis of the lagging DNA strand of simian virus 40. J. Virol. **64:**5912–5918.
52. **Patel, S. S., and K. M. Picha.** 2000. Structure and function of hexameric helicases. Annu. Rev. Biochem. **69:**651–697.
53. **Paucha, E., D. Kalderon, R. W. Harvey, and A. E. Smith.** 1986. Simian virus 40 origin DNA-binding domain on large T antigen. J. Virol. **57:**50–64.
54. **Peden, K. W. C., and J. M. Pipas.** 1985. Site-directed mutagenesis of the simian virus 40 large T-antigen gene: replication-defective amino acid substitution mutants that retain the ability to induce morphological transformation. J. Virol. **55:**1–9.
55. **Pervushin, K. V., R. Riek, G. Wider, and K. Wuthrick.** 1997. Attenuated T2 relaxation by mutual cancellation of dipole-dipole coupling and chemical shift anisotropy indicates an avenue to NMR structures of very large biological macromolecules in solution. Proc. Acad. Natl. Sci. USA **94:**12366–12371.
56. **Prives, C., L. Covey, A. Scheller, and Y. Gluzman.** 1983. DNA-binding properties of simian virus 40 T-antigen mutants defective in viral DNA replication. Mol. Cell. Biol. **3:**1958–1966.
57. **Purviance, J. D., A. E. Prack, B. A. Barbaro, and P. A. Bullock.** 2001. In the simian virus 40 in vitro replication system, start site selection by the polymerase α-primase complex is not significantly altered by changes in the concentration of ribonucleotides. J. Virol. **74:**6392–6401.
58. **Ray, S., M. E. Anderson, G. Loeber, D. McVey, and P. Tegtmeyer.** 1992. Functional characterization of temperature-sensitive mutants of simian virus 40 large T antigen. J. Virol. **66:**6509–6516.
59. **Reese, D. K., K. R. Sreekumar, and P. A. Bullock.** 2004. Interactions required for binding of simian virus 40 T antigen to the viral origin and molecular modeling of initial assembly events. J. Virol. **78:**2921–2934.
60. **Richardson, J. P.** 2003. Loading Rho to terminate transcription. Cell **114:**157–159.
61. **Robinson, C. G., and J. M. Pipas.** 1998. SV40 large turmor antigen (T antigen): database of mutants. Nucleic Acids Res. **26:**295–296.
62. **Rutila, J. E., M. J. Imperiale, and W. W. Brockman.** 1986. Replication and transformation functions of in vitro generated simian virus 40 large T-antigen mutants. J. Virol. **58:**526–535.
63. **San Martin, M. C., C. Gruss, and J. M. Carazo.** 1997. Six molecules of SV40 large T antigen assemble in a propeller-shaped particle around a channel. J. Mol. Biol. **268:**15–20.
64. **Schuck, S., and A. Stenlund.** 2005. Assembly of a double hexamer helicase. Mol. Cell **20:**377–389.
65. **Shen, J., D. Gai, A. Patrick, W. B. Greenleaf, and X. S. Chen.** 2005. The roles of the residues on the channel β-hairpin and loop structures of simian virus 40 hexameric helicase. Proc. Natl. Acad. Sci. USA **102:**11248–11253.
66. **Simmons, D. T.** 2000. SV40 Large T antigen functions in DNA replication and transformation. Adv. Virus Res. **55:**75–134.
67. **Simmons, D. T., G. Loeber, and P. Tegtmeyer.** 1990. Four major sequence elements of simian virus 40 large T antigen coordinate its specific and nonspecific DNA binding. J. Virol. **64:**1973–1983.
68. **Simmons, D. T., R. Upson, K. Wun-Kim, and W. Young.** 1993. Biochemical analysis of mutants with changes in the origin-binding domain of simian virus 40 tumor antigen. J. Virol. **67:**4227–4236.
69. **Simmons, D. T., K. Wun-Kim, and W. Young.** 1990. Identification of simian virus 40 T-antigen residues important for specific and nonspecific binding to DNA and for helicase activity. J. Virol. **64:**4858–4865.
70. **Singleton, M. R., M. S. Dillingham, M. Gaudier, S. C. Kowalczykowski, and D. B. Wigley.** 2004. Crystal structure of RecBCD enzyme reveals a machine for processing DNA breaks. Nature **432:**187–193.
71. **Skordalakes, E., and J. M. Berger.** 2003. Structure of the Rho transcription terminator: mechanism of mRNA recognition and helicase loading. Cell **114:**135–146.
72. **Smelkova, N. V., and J. A. Borowiec.** 1997. Dimerization of simian virus 40 T-antigen hexamers activates T-antigen DNA helicase activity. J. Virol. **71:**8766–8773.
73. **Spillman, T., D. Giacherio, and L. P. Hager.** 1979. Single strand DNA binding of simian virus 40 tumor antigen. J. Biol. Chem. **254:**3100–3104.
74. **Stahl, H., P. Droge, and R. Knippers.** 1986. DNA helicase activity of SV40 large tumor antigen. EMBO J. **5:**1939–1944.
75. **Stenlund, A.** 2003. Initiation of DNA replication: lessons from viral initiator proteins. Nat. Rev. **4:**777–785.
76. **Stillman, B., R. D. Gerard, R. A. Guggenheimer, and Y. Gluzman.** 1985. T antigen and template requirement for SV40 DNA replication in vitro. EMBO J. **4:**2933–2939.
77. **Stringer, J. R.** 1982. Mutant of simian virus 40 large T-antigen that is defective for viral DNA synthesis, but competent for transformation of cultured rat cells. J. Virol. **42:**854–864.
78. **Titolo, S., E. Welchner, P. W. White, and J. Archambault.** 2003. Characterization of the DNA-binding properties of the origin-binding domain of SV40 large T antigen by fluorescence anisotropy. J. Virol. **77:**5512–5518.
79. **Tye, B. K., and S. Sawyer.** 2000. The hexameric eukaryotic MCM helicase: building symmetry from nonidentical parts. J. Biol. Chem. **275:**34833–34836.
80. **Valle, M., X. S. Chen, L. E. Donate, E. Fanning, and J. M. Carazo.** 2006. Structural basis for the cooperative assembly of large T antigen on the origin of replication. J. Mol. Biol. **357:**1295–1305.
81. **Valle, M., C. Gruss, L. Halmer, J. M. Carazo, and L. E. Donate.** 2000. Large T-antigen double hexamers imaged at the simian virus 40 origin of replication. Mol. Cell. Biol. **20:**34–41.
82. **van Brabant, A. J., R. Stan, and N. A. Ellis.** 2000. DNA helicases, genomic instability, and human genetic disease. Annu. Rev. Genom. Hum. Genet. **1:**409–459.
83. **VanLoock, M. S., A. Alexandrov, X. Yu, N. R. Cozzarelli, and E. H. Egelman.** 2002. SV40 large T antigen hexamer structure: domain organization and DNA-induced conformational changes. Curr. Biol. **12:**472–476.
84. **Waga, S., and B. Stillman.** 1998. The DNA replication fork in eukaryotic cells. Annu. Rev. Biochem. **67:**721–751.
85. **Weisshart, K., P. Taneja, and E. Fanning.** 1998. The replication protein A binding site in simian virus 40 (SV40) T antigen and its role in the initial steps of SV40 DNA replication. J. Virol. **72:**9771–9781.
86. **Weisshart, K., P. Taneja, A. Jenne, U. Herbig, D. T. Simmons, and E. Fanning.** 1999. Two regions of simian virus 40 T antigen determine cooperativity of double-hexamer assembly on the viral origin of DNA replication and promote hexamer interactions during bidirectional origin DNA unwinding. J. Virol. **73:**2201–2211.
87. **Welsh, J. D., C. Swimmer, T. Cocke, and T. Shenk.** 1986. A second domain of simian virus 40 T antigen in which mutations can alter the cellular localization of the antigen. Mol. Cell. Biol. **6:**2207–2212.
88. **Wessel, R., J. Schweizer, and H. Stahl.** 1992. Simian virus 40 T-antigen DNA helicase is a hexamer which forms a binary complex during bidirectional unwinding from the viral origin of DNA replication. J. Virol. **66:**804–815.
89. **Wold, M. S.** 1997. Replication protein A: a heterotrimeric, single-stranded DNA-binding protein required for eukaryotic DNA metabolism. Annu. Rev. Biochem. **66:**61–92.
90. **Wold, M. S., J. J. Li, and T. J. Kelly.** 1987. Initiation of simian virus 40 DNA replication in vitro: large-tumor-antigen- and origin-dependent unwinding of the template. Proc. Natl. Acad. Sci. USA **84:**3643–3647.
91. **Wu, C., R. Roy, and D. T. Simmons.** 2001. Role of single-stranded DNA binding activity of T antigen in simian virus 40 DNA replication. J. Virol. **75:**2839–2847.
92. **Wun-Kim, K., and D. T. Simmons.** 1990. Mapping of helicase and helicase substrate-binding domains on simian virus 40 large T antigen. J. Virol. **64:**2014–2020.
93. **Wun-Kim, K., R. Upson, W. Young, T. Melendy, B. Stillman, and D. T. Simmons.** 1993. The DNA-binding domain of simian virus 40 tumor antigen has multiple functions. J. Virol. **67:**7608–7611.
94. **Yuzhakov, A., Z. Kelman, J. Hurwitz, and M. O'Donnell.** 1999. Multiple competition reactions for RPA order the assembly of the DNA polymerase δ holoenzyme. EMBO J. **18:**6189–6199.